Macromolecular Bioscience
www.mbs-journal.de

Calcium Signaling Regulates Valvular Interstitial Cell Alignment and Myofibroblast Activation in Fast-Relaxing Boronate Hydrogels

*Hao Ma, Laura J. Macdougall, Andrea Gonzalez Rodriguez, Megan E. Schroeder, Dilara Batan, Robert M. Weiss, and Kristi S. Anseth**

The role viscoelasticity in fibrotic disease progression is an emerging area of interest. Here, a fast-relaxing hydrogel system is exploited to investigate potential crosstalk between calcium signaling and mechanotransduction. Poly(ethylene glycol) (PEG) hydrogels containing boronate and triazole crosslinkers are synthesized, with varying ratios of boronate to triazole crosslinks to systematically vary the extent of stress relaxation. Valvular interstitial cells (VICs) encapsulated in hydrogels with the highest levels of stress relaxation (90%) exhibit a spread morphology by day 1 and are highly aligned (80 ± 2%) by day 5. Key myofibroblast markers, including α-smooth muscle actin (αSMA) and collagen 1a1 (COL1A1), are significantly elevated. VIC myofibroblast activation decreases by 42 ± 18% through inhibition of mechanotransduction, independently of VIC morphology and alignment. Calcium signaling through a transient receptor potential vanilloid 4 (TRPV4) is found to regulate VIC spreading, alignment, and activation in a time dependent manner. Inhibition of calcium signaling at early time points results in disturbed cell alignment, decreased mechanotransduction, and diminished activation, while inhibition at later time points only causes partially reduced myofibroblast activation. These results suggest a potential crosstalk mechanism, where calcium signaling acts upstream of mechanosensing and can regulate VIC myofibroblast activation independently of mechanotransduction.

1. Introduction

Aortic valve stenosis (AVS) is a progressive disease that is characterized by poorly functioning, calcified valve leaflets that ultimately impede proper blood flow through the heart.[1,2] There are no therapies known to inhibit the progression of AVS, necessitating over 100 000 valve replacement procedures in the US annually.[3,4] The valvular interstitial cell (VIC) is the most abundant cell type that resides in the heart valve and is a regulator of valvular tissue homeostasis.[5] Upon injury or in the presence of inflammatory cues in the valve, VICs can transition from a quiescent fibroblast phenotype into an activated myofibroblast phenotype,[5–7] characterized by α-smooth muscle actin (αSMA) stress fibers and increased deposition of collagen fibers into the extracellular matrix (ECM).[8,9] Persistent VIC activation can lead to a stiff and disorganized collagen matrix in valve leaflets, which is associated with valvular fibrosis and can ultimately result in AVS, when left untreated.[9]

Diseased valvular tissue can be evaluated in many ways, including histologic assessment of structural changes and increased calcium deposition.[10–12] For example, collagen fibers, which are the main structural component of the heart valve matrix, can reorganize in a diseased state, significantly altering the mechanical properties and function of the leaflets resulting in VIC activation and altered functions.[10,13] The orientation of collagen fibers is highly associated with

Dr. H. Ma, Dr. L. J. Macdougall, Dr. A. Gonzalez Rodriguez, Prof. K. S. Anseth
Department of Chemical and Biological Engineering
University of Colorado Boulder
Boulder, CO 80303, USA
E-mail: kristi.anseth@colorado.edu

Dr. H. Ma, Dr. L. J. Macdougall, Dr. A. Gonzalez Rodriguez, Dr. M. E. Schroeder, D. Batan, Prof. K. S. Anseth
The BioFrontiers Institute
University of Colorado Boulder
Boulder, CO 80303, USA

The ORCID identification number(s) for the author(s) of this article can be found under https://doi.org/10.1002/mabi.202000268.

DOI: 10.1002/mabi.202000268

Dr. M. E. Schroeder
Materials Science and Engineering Program
University of Colorado Boulder
Boulder, CO 80303, USA

D. Batan
Department of Biochemistry
University of Colorado Boulder
Boulder, CO 80303, USA

Prof. R. M. Weiss
Division of Cardiovascular Medicine
University of Iowa
Iowa City, IA 52242, USA

the orientation of VICs, and therefore, VIC alignment is a key indicator of disease progression.[14–16] However, how VIC alignment influences myofibroblast activation and other VIC functions remain largely unknown. Calcium signaling has also been linked to disease progression, especially collagen organization during fibrosis development.[17–19] For instance, the Chaudhuri group demonstrated that the mechanoresponsive transient receptor potential vanilloid 4 (TRPV4) channel can regulate mesenchymal stem cell spreading and osteogenic differentiation when cultured in 3D viscoelastic material systems.[20] TPRV4 channels have also been found to regulate dermal, pulmonary, and cardiac fibroblast activation in response to both mechanical and biochemical stimuli.[21–24] However, the specific role that TRPV4 activity plays in VIC myofibroblast activation has been less explored. We propose a controlled in vitro material system with tunable viscoelasticity, allowing for a deeper understanding into the mechanism of cell alignment and calcium signaling, and their relationship to VIC activation that correlates with valve disease progression.

Ideally, mechanosensing of VICs cultured in a 3D biomaterial culture system should reflect the properties of diseased valve tissue. Enhanced collagen deposition during disease progression not only increases the stiffness of extracellular matrix, but also alters its viscoelastic properties.[12,25] Viscoelasticity is a time-dependent mechanical property, and there is a growing appreciation for the role viscoelasticity plays in influencing cell fate decisions.[26–31] Healthy heart valves are viscoelastic and can relax up to 30% of applied stresses;[32] however, during the progression of AVS, the ability for the valve to relax stresses dynamically changes.[25,33]

Within the past decade, numerous hydrogel scaffolds with time-dependent mechanical properties have been reported in the literature and used to investigate the effect of viscoelasticity on various cell types.[29–31,34] For example, Cameron et al. varied the crosslinking density of poly(acrylamide) gels to control the creep response and showed that the spreading and proliferation of human mesenchymal stem cells (hMSCs) increased with the viscous (loss) modulus.[30] Later, Mooney and co-workers controlled the relaxation rate of alginate hydrogels by changing the polymer molecular weight and binding affinity of the calcium chelating domains.[26] Using this material system to encapsulate hMSCs, the authors demonstrated that stress relaxation promoted the formation of stress fibers, focal adhesions, mechanotransduction, and even osteogenic differentiation.[29] Covalently adaptable networks (CANs), hydrogel network structures crosslinked with a sufficient number of reversible covalent bonds, have also shown great promise to effectively tune viscoelastic properties.[35] McKinnon et al. demonstrated that CANs can be designed with controlled elastic moduli and stress relaxation time constants while being cytocompatible for myoblast encapsulation.[36] Boronate crosslinks between a boronic acid and diol have shown many potential applications for glucose sensor, drug delivery, and self-healing materials,[37–40] although limited applications were achieved for stable cell culture scaffolds.[37,41] Tang et al. developed covalent adaptable poly(ethylene glycol) hydrogels by screening boronate crosslinks formed by a range of different boronic acids and diols to achieve tunable rates of stress relaxation.[31] This material was fast-relaxing (e.g., relaxation time constant ranges from 0.1 to 1 s) and stable for long-term cell culture with the incorporation of permanent strain-promoted azide-alkyne cycloaddition (SPAAC) bonds.[31] This hydrogel platform was further used to study the effect of mechanotransduction and Yes-associated protein and its transcriptional coactivator with PDZ-binding motif (YAP/TAZ) signaling on encapsulated hMSCs.[31] Computational analysis of cell-matrix interaction within these networks has shown to predict cell spreading upon substrate relaxation are maximized when the networks have comparable timescales to integrin clutch binding on the cell surface.[42]

As the fast relaxing boronate hydrogel system has been shown to have similar relaxation time constants to cell-matrix interactions,[31,42] this system was chosen to examine the role that viscoelasticity plays on VIC cellular responses in 3D microenvironments. The covalently adaptable network includes nondynamic triazole bonds and dynamic boronate bonds. The percentage of dynamic boronate bonds was systematically varied in the final gel formulation to create hydrogel scaffolds with different percentages of stress relaxation. VICs were cultured in hydrogel scaffolds with none, low, medium and high percentage of stress relaxation, and the effect of viscoelasticity on VIC myofibroblast activation was examined. VIC spreading, alignment, and myofibroblast activation were monitored with respect to manipulation of mechanotransduction pathways and mechanoresponsive calcium channels. Based on the results of this study, TRPV4 calcium signaling was proposed to act upstream of YAP/TAZ mechanotransduction and also capable of regulating VIC myofibroblast activation independently of mechanotransduction. Overall, this study demonstrates how 3D in vitro culture scaffolds with systematically controlled viscoelasticity can be exploited to study the mechanism of VIC response to time-dependent matrix mechanical properties. A better understanding of such process will aid in better design of tissue regenerative scaffolds as well as medical treatments for valvular tissue fibrosis.

2. Results

2.1. Development of Hydrogel Formulation with Extents of Relaxation

To investigate the effect of viscoelasticity on VIC myofibroblast activation, hydrogels scaffolds with different stress relaxation properties were developed. Specifically, viscoelastic hydrogel systems were formed through two crosslinking chemistries, a permanent triazole bond through a SPAAC reaction between a dibenzylcyclooctyne (DBCO) group and an azide and a reversible boronate bond between a diol, nitrodopamine (ND), and a boronic acid, 2-fluorophenylboronic acid (FPBA) (**Figure 1**A). This system was chosen after previous studies showed similar relaxation time constants that promote cell–matrix interactions[31,42] Briefly, octa-arm poly(ethylene glycol) (PEG)-DBCO was mixed with octa-arm PEG-ND/azide and PEG-FPBA/azide (or PEG-Azide for elastic hydrogel formula) at different ratios to control the viscoelastic properties. The more reversible bond (e.g., boronate bonds) in the system,

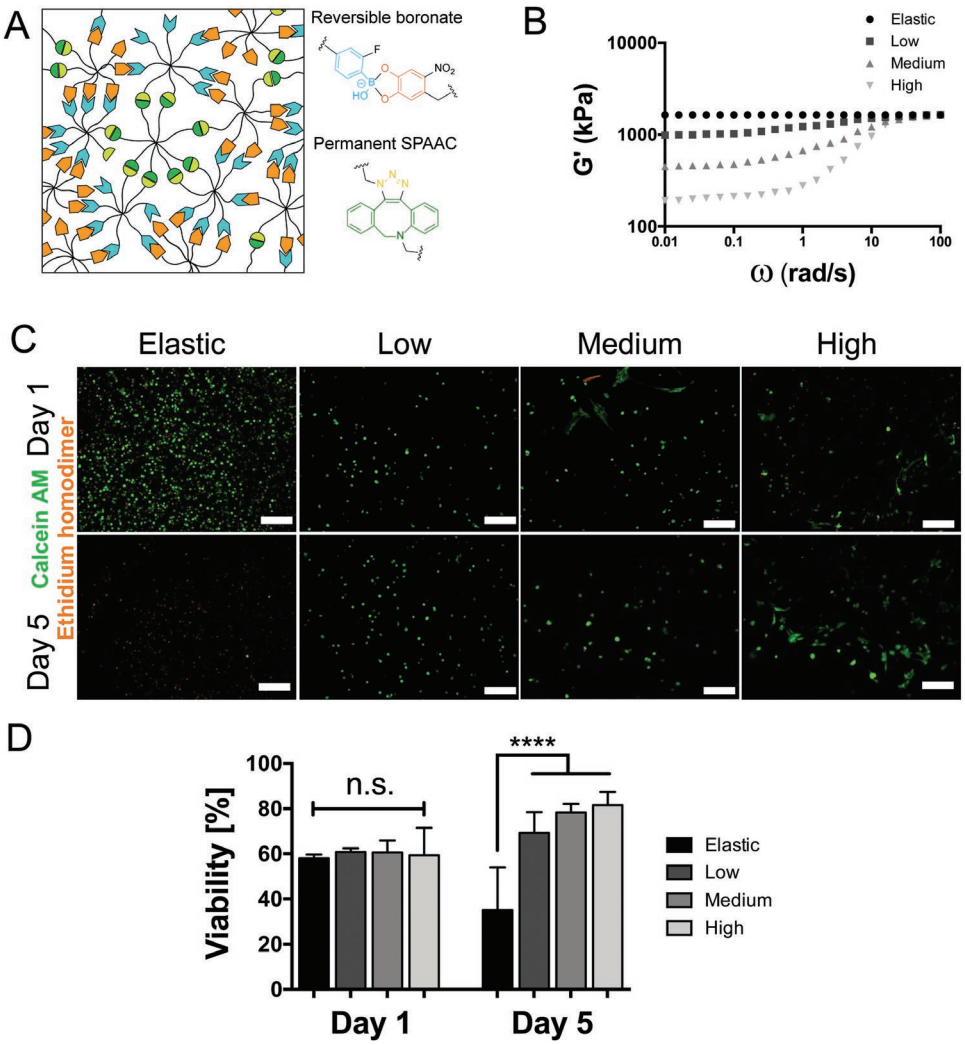

Figure 1. Development of hydrogel formulations with different extents of stress relaxation. A) Schematic of hydrogel scaffolds containing both reversible boronate bonds and permanent SPAAC bonds. Reproduced with permission.[24] Copyright 2018, Wiley-VCH GmbH. B) Representative frequency sweeps of hydrogels containing different percentage of boronate crosslinkers, leading to different relaxation behaviors. Measurements were performed at 37 °C. C) Representative live/dead images of male VICs cultured in different hydrogel formulations at Day 1 and Day 5 post encapsulation. Live cells were stained with calcium AM (green) and dead cells were stained with ethidium homodimer (orange). D) Quantification of VICs viability encapsulated in different hydrogel formulations at Day 1 and Day 5. Values are plotted as mean ± standard deviation. n.s.: $p > 0.05$, ****: $p < 0.0001$, based on one-way ANOVA. Three biological replicates with three technical replicates in each biological replicate, at least 200 VICs were analyzed per technical replicate. Scale bar = 200 µm.

the higher percentage of viscoelasticity the system exhibits. Four formulas were developed with different percentages of reversible boronate bonds, 0% (elastic, no reversible boronate bonds), 20% (low), 40% (medium), or 60% (high) and gelation occurred in under 15 min (Figure 1B, **Table 1**; and Table S1, Supporting Information). The same high frequency plateau modulus G′∞ (1.6 ± 0.2 kPa) was observed for all four formulas from rheological frequency sweep measurements, and different moduli after relaxation G′0 were observed: 1.6 ± 0.2 kPa for elastic formula, 1.0 ± 0.2 kPa for low formula, 0.5 ± 0.1 kPa for medium formula, and 0.2 ± 0.1 for high formula, which corresponds to relaxation percentages around 0%, 40%, 70% or 90%, respectively. By systematically varying the viscoelastic properties of these hydrogels, the range of viscoelasticity that can be achieved is vast, e.g., tissue specific properties for valvular tissue at different stages of fibrotic and calcific disease progression.[12] For this study, we were interested in the effect that changes in viscoelasticity would have on VIC phenotype, rather than matching the stress relaxation of heart value tissue. Therefore, these stress relaxation values enable us to understand and explore this characteristic under a range of different settings. To test the viability of VICs in different hydrogel formulas, live and dead staining was performed on male porcine-derived VICs encapsulated at 1×10^7 cell mL^{-1} in the different formulations at day 1 and day 5 postencapsulation. The large number of cells required to perform these 3D culture experiments, together with the limited ability to passage primary cells in vitro while maintaining their fibroblast properties, limited the practical use of human VICs. Therefore, porcine-derived VICs were utilized for this study.

Table 1. Summary of the hydrogel formulations and mechanical properties for each formula. The percentage of boronate crosslinkers and mechanical properties measured by rheological frequency sweep for each formula were summarized in Table 1. The percentage of stress relaxation for each formula was calculated by $(G'_{\infty} - G'_0)/G'_{\infty}$.

Formulas with different amount of dynamic bonds	Elastic	Low	Medium	High
Percentage of boronate crosslinkers [%]	0	20	40	60
G'_{∞} [kPa]	1.6 ± 0.2	1.6 ± 0.2	1.6 ± 0.2	1.6 ± 0.2
G'_0 [kPa]	1.6 ± 0.2	1.0 ± 0.2	0.5 ± 0.1	0.2 ± 0.1
Stress relaxation [%]	≈0	≈40	≈70	≈90

All hydrogel formulas had an azide functionalized fibronectin-mimicking peptide GRGDS incorporated at a concentration of 3×10^{-3} M to promote cell-matrix adhesion. The viability of VICs at day 1 in all four formulas was similar (elastic: 58 ± 2%, low: 61 ± 2%, medium: 61 ± 5%, high: 59 ± 12%, Figure 1C,D). However, by day 5, viability had increased for the low (69 ± 9%), medium (78 ± 4%), and high (82 ± 6%) formulas, but notably decreased (35 ± 19%) for VICs cultured in elastic formula with no boronate linkages (Figure 1C,D). This loss in viability was attributed to the lack of matrix remodeling and cell spreading in purely elastic hydrogel system without dynamic bonds.[43] Therefore, only low, medium, and high formulas were used in following experiments to further elucidate the effect of viscoelasticity on VIC cellular responses.

2.2. VIC Spreading and Myofibroblast Activation is Affected by Viscoelasticity

VICs cultured in low, medium, and high viscoelastic hydrogel formulas exhibited distinguishable morphological differences after 1 day postencapsulation and such differences became more dramatic by day 5 (**Figure 2**A). At day 1, VICs cultured in low and medium formulas only exhibited modest protrusions into the matrix, whereas the VICs cultured in high relaxing formulas, where the boronate crosslinks allowed high levels of stress relaxation, exhibited extensive spreading. The morphological differences were further quantified at day 5, VICs cultured in high relaxing formulas exhibited an elongated morphology and had significantly higher alignment of nuclei (80 ± 2%) compared to low (17 ± 5%) and medium (18 ± 6%) viscoelastic hydrogel (Figure 2B). Myofibroblast activation of VICs was evaluated in these same formulas by quantifying the immunostained αSMA intensity and gene expression level of key myofibroblast markers (αSMA (ACTA2) and collagen 1a1 (COL1A1)). VICs cultured in the high formula had a sevenfold increase in the immunostained αSMA intensity compared to VIC cultured in low and medium formulas, indicating VICs activated into myofibroblast in the highly viscoelastic networks by day 5 (Figure 2C,D). Consistent with the immunostaining analysis of αSMA protein, VICs cultured in the highly viscoelastic systems also exhibited elevated expression of key myofibroblast markers (around a 16-fold increase for αSMA and fivefold increase for COL1A1), based on real-time polymerase chain reaction (RTq-PCR) quantification (Figure 2E). Such dramatic changes of VIC morphology and activation indicates the important effects of viscoelasticity on VIC cellular response during fibrotic disease progression. To further confirm phenotypic changes in VICs in high stress relaxing formulas at day 5, FGF-2, a mitogen effector that maintains the quiescent VIC fibroblast phenotype,[44] was delivered to VICs cultured in these systems. When FGF-2 was presented at a concentration over 10 ng mL^{-1}, VICs exhibited a significant decrease in immunostained αSMA intensity by 74 ± 9% compared to control groups without FGF-2 treatment (**Figure 3**A,B). Such effect of FGF-2 on VIC phenotypic change was also confirmed by quantifying the change of ACTA2 and COL1A1 gene expression with 10 ng mL^{-1} FGF-2 treatment. Both genes had significantly decreased expression levels compared to the nontreated control group, as quantified by RTq-PCR analyses (Figure 3C). VIC spreading and nuclear alignment cultured in the highest relaxation formula was not affected by FGF-2 treatments, indicating a mechanism where FGF-2 affects VIC myofibroblast activation independently of VIC morphology (Figure 3D).

2.3. VIC Mechanotransduction is Affected by Viscoelasticity and Regulates VIC Myofibroblast Activation

To investigate how mechanotransduction is affected by different percentages of stress relaxation, YAP/TAZ subcellular localization was quantified using immunostained VICs cultured in low, medium, and high formulas. VICs encapsulated in high viscoelastic networks exhibited a significantly higher nuclear to cytoplasm ratio of YAP/TAZ (2.5 ± 0.4), compared to VICs in low and medium viscoelastic systems (low: 1.4 ± 0.1, medium: 1.4 ± 0.3). These results suggest that this mechanotransduction pathway is more activated for VICs cultured in 3D systems that allow a high level of stress relaxation (**Figure 4**A,B). To further examine the role of mechanotransduction on VIC spreading, alignment, and myofibroblast activation, verteporfin (VP), an inhibitor of YAP/TAZ nuclear shuttling, was delivered to VICs cultured in the high viscoelastic formulas. The YAP/TAZ nuclear to cytoplasm ratio was significantly decreased from 2.5 ± 0.4 to 1.8 ± 0.2 by the inhibitor treatment (Figure 4C,D). Inhibition of YAP/TAZ nuclear localization significantly decreased the immunostained αSMA intensity by 42 ± 18% (Figure 4E,F), indicating a diminished myofibroblast phenotypic change of VICs with YAP/TAZ nuclear shuttling inhibition. However, VIC cell spreading and nuclear alignment were not influenced by inhibition of YAP/TAZ nuclear shuttling as quantified by immunostained images (Figure 4D,F,G).

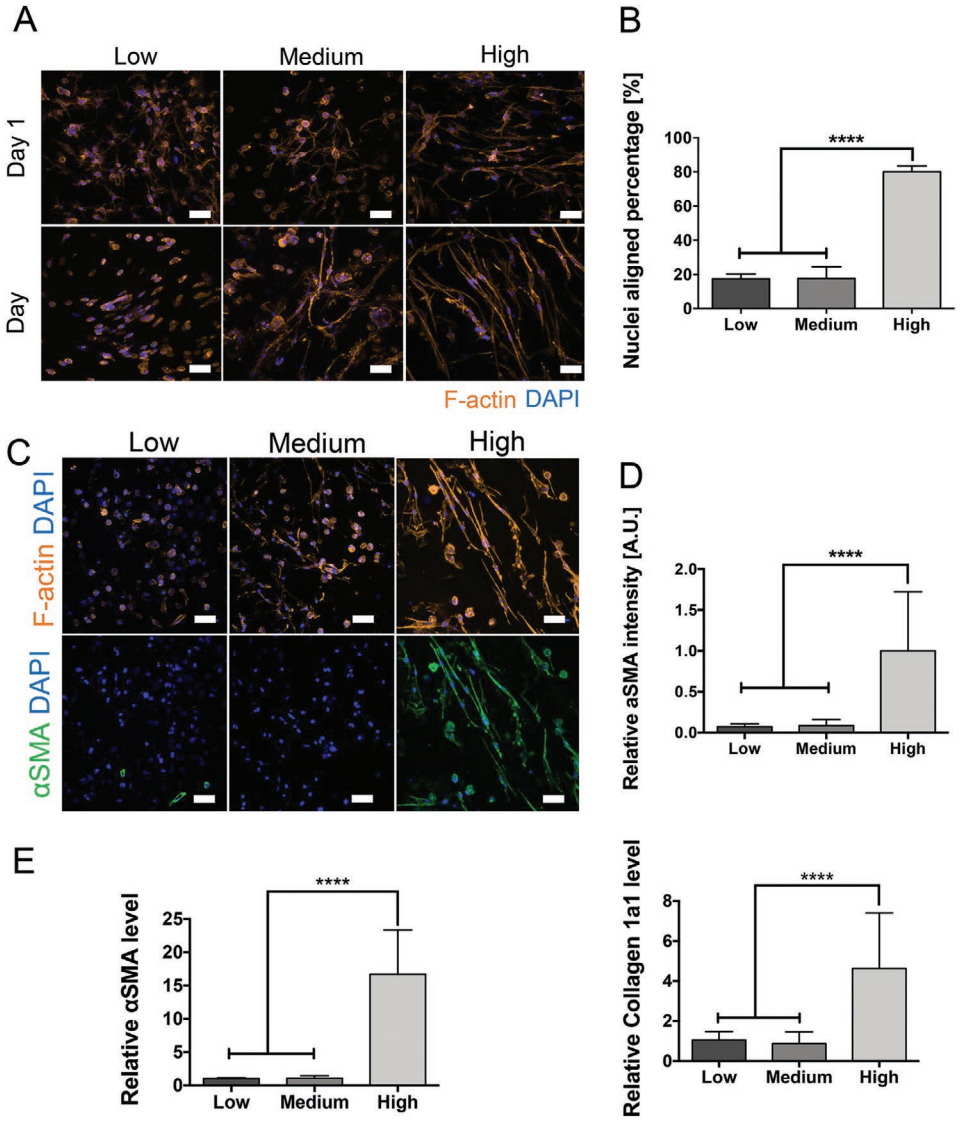

Figure 2. VIC spreading and myofibroblast activation depend on viscoelasticity. A) Representative immunostaining images for nuclei (blue) and F-actin (orange) of VICs cultured in different viscoelastic hydrogel formulas at Day 1 and Day 5. B) Quantification of nuclear alignment of VICs encapsulated in different viscoelastic hydrogel formulations at Day 5. C) Representative immunostaining images of nuclei (blue), F-actin (orange), and αSMA stress fibers (green) of VICs cultured in different viscoelastic hydrogel formulations at Day 5. D) Quantification of αSMA intensity for VICs encapsulated in different hydrogel formulations. E) Relative mRNA expression levels normalized to L30 of key myofibroblast markers, αSMA and COL1A1, for VICs cultured in different hydrogel formulations. Values are plotted as mean ± standard deviation. ****: $p < 0.0001$, based on one-way ANOVA. Three biological replicates with three technical replicates in each biological replicate, at least 200 VICs were analyzed per technical replicate. Scale bar = 50 µm.

2.4. TRPV4 Activities are Involved in VIC Spreading and Myofibroblast Activation

As calcium signaling plays an important role in mechanotransduction, the calcium levels for VICs cultured in low, medium, and high viscoelastic formulas were measured.[45] VICs in highly viscoelastic networks exhibited a twofold increase in intracellular calcium levels, compared to VICs cultured in lower viscoelastic formulas (Figure S1A,B, Supporting Information). As TRPV4, a calcium permeable channel, has been shown to play a role in mechanotransduction,[46] its involvement during VIC myofibroblast activation was further examined. A TPRV4 antagonist, GSK 2193874,[47] that has been proven to inhibit TRPV4 activities specifically, was used to further elucidate the role TRPV4 plays in VIC spreading and myofibroblast activation. When TRPV4 antagonist was presented at a concentration over 1000×10^{-9} M at day 1, the immunostained αSMA intensity of VICs in the high formula hydrogels significantly decreased by 71 ± 9% compared to the nontreated control group at day 5 (**Figure 5**A). More interestingly, VIC became more rounded, and the nuclear alignment was also diminished (from 80 ± 3% to 14 ± 2%) upon treatment with the TRPV4 antagonist at concentrations over 1000×10^{-9} M from day 1 to day 5 (Figure 5B,E). In order to confirm the changes in VIC morphology and activation were not a result of cell death, VIC viability was measured. No significant differences were observed with TRPV4 antagonist

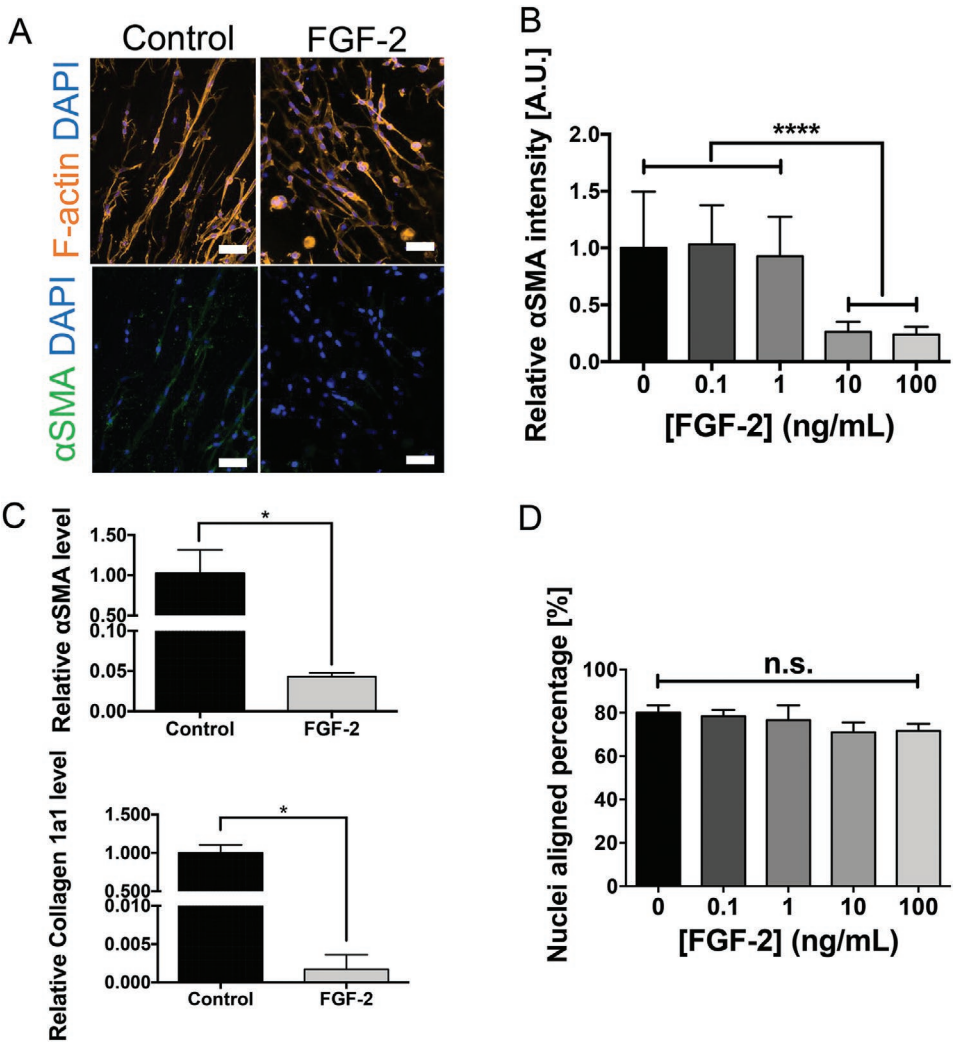

Figure 3. VIC myofibroblast activation responds to FGF-2 treatment within high viscoelastic hydrogel system. A) Representative immunostaining images of nuclei (blue), F-actin (orange), and αSMA stress fibers (green) of VICs cultured within hydrogels with the highest percent of boronate crosslinkers in the presence or absence of FGF-2 (10 ng mL^{-1}) treatment at Day 5. B) Quantification of αSMA intensity of VICs encapsulated within high viscoelastic hydrogels in response to a range of FGF-2 concentrations (0, 0.1, 1, 10, and 100 ng mL^{-1}) at Day 5. C) mRNA relative expression levels normalized to L30 of key myofibroblast markers, αSMA and COL1A1, for VICs cultured within high viscoelastic hydrogels in the presence or absence of FGF-2 (10 ng mL^{-1}) treatment. D) Quantification of nuclear alignment percentage of VICs encapsulated in the high viscoelastic system in response to different concentrations of FGF-2 (0, 0.1, 1, 10, and 100 ng mL^{-1}) at Day 5. Values are plotted as mean ± standard deviation. *: $p < 0.05$, ****: $p < 0.0001$, based on one-way ANOVA. Three biological replicates with three technical replicates in each biological replicate, at least 200 VICs were analyzed per technical replicate. Scale bar = 50 µm.

treatment up to 1000×10^{-9} M (Figure S2, Supporting Information). Therefore, 1000×10^{-9} M of TRPV4 antagonist was selected as the dosing concentration for subsequent studies. Such phenotypic changes in VICs upon TRPV4 antagonist treatment were further confirmed by quantification of the gene expression levels of ACTA2 and COL1A1, both of which exhibited significant decreases upon TRPV4 antagonist treatment (Figure 5C). The TRPV4 antagonist was also delivered to VICs in high viscoelastic formula hydrogels at day 4 for an additional day, until day 5, in order to further investigate the role of TRPV4 activity in VIC myofibroblast activation in addition to cell spreading. VICs cultured in high viscoelastic networks already exhibited a spread cell morphology and nuclear alignment at day 4, and as such, a spread cell morphology and nuclear alignment were not influenced by an additional day of TPRV4 treatment (Figure 5D). However, a partial decrease (38 ± 12%) in αSMA intensity was observed with TPRV4 antagonist treatment and via immunostaining analysis between day 4 and day 5.

2.5. Crosstalk Between Mechanotransduction and TRPV4 Activity Regulates VIC Myofibroblast Activation

As a mechanosensitive calcium permeable cation channel, TPRV4 activity has been shown to regulate mechanotransduction via YAP/TAZ nuclear shutting mechanism in various cell types, such as mesenchymal stem cell, lung fibroblast, and cardiac fibroblast.[20,22,48–50] The YAP/TAZ subcellular localizations were characterized at different time points for VICs cultured in viscoelastic networks upon TRPV4 antagonist treatment at

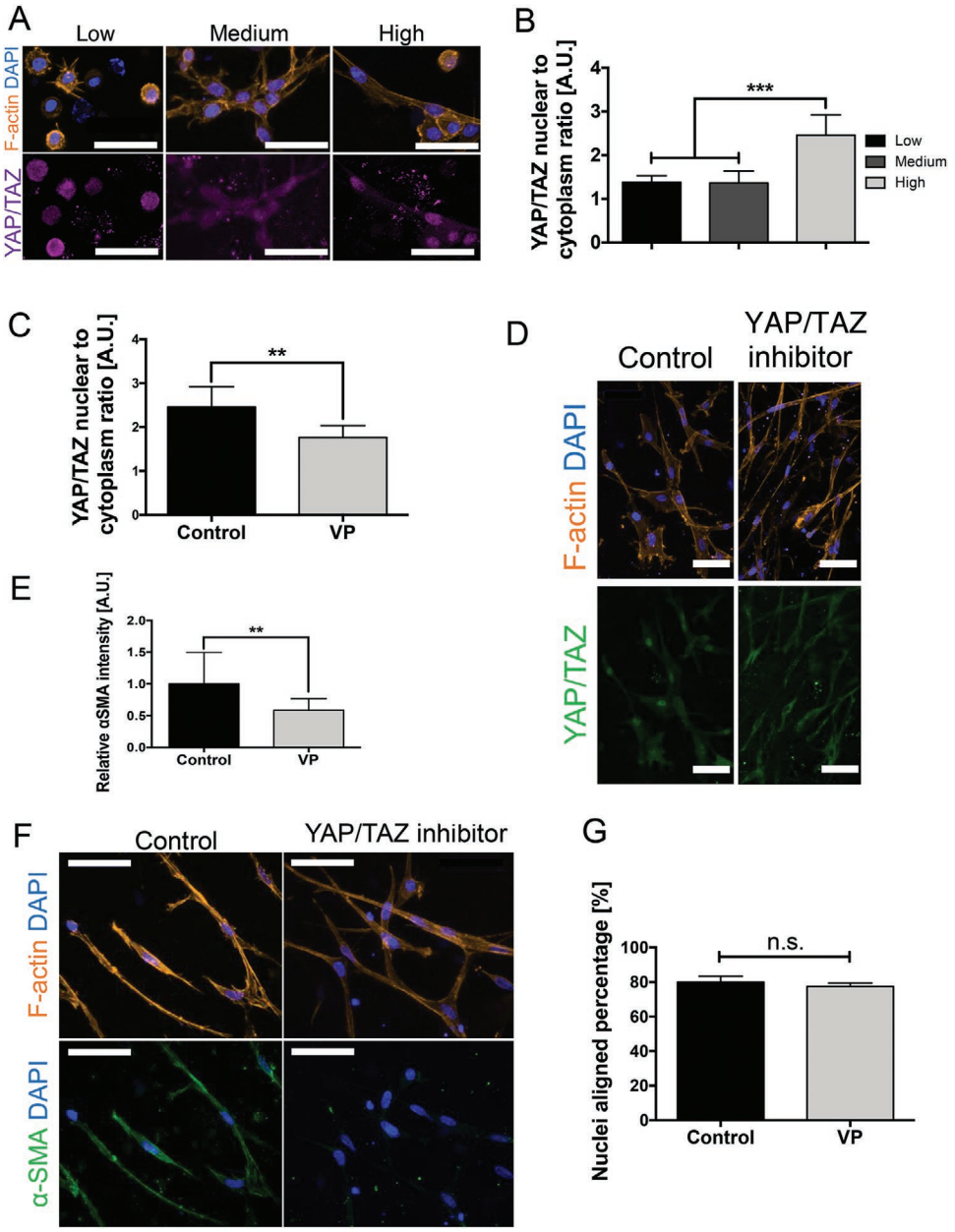

Figure 4. VIC mechanotransduction depends on viscoelasticity of the hydrogel and regulates VIC myofibroblast activation. A) Representative immunostaining images of nuclei (blue), F-actin (orange), and YAP/TAZ (purple) of VICs cultured in different viscoelastic hydrogel formulations at Day 2. B) Quantification of the YAP/TAZ nuclear to cytoplasm ratio for VICs cultured in different viscoelastic formulations at Day 2. C) Quantification of YAP/TAZ nuclear to cytoplasm ratio for VICs cultured in high viscoelastic system with or without 3×10^{-6} M YAP/TAZ inhibitor (VP) treatment at Day 2. D) Representative immunostaining images of nuclei (blue), F-actin (orange), and YAP/TAZ (green) of VIC cultured in the high viscoelastic formulation with or without YAP/TAZ inhibitor (VP) at Day 5. E) Quantification of αSMA intensity for VICs cultured in the high viscoelastic system with or without YAP/TAZ inhibitor treatment (VP) at Day 5. F) Representative immunostaining images of nuclei (blue), F-actin (orange), and αSMA (green) of VICs cultured in the high viscoelastic system with or without YAP/TAZ inhibitor treatment (VP) at Day 5. G) Quantification of nuclear alignment of VIC cultured within high viscoelasticity hydrogels with or without YAP/TAZ inhibitor treatment (VP) at Day 5. Values are plotted as mean ± standard deviation. n.s.: $p > 0.05$, **: $p < 0.01$, ***: $p < 0.001$, based on one-way ANOVA. Three biological replicates with three technical replicates in each biological replicate, at least 200 VICs were analyzed per technical replicate. Scale bar = 50 μm.

day 1. YAP/TAZ nuclear to cytoplasm ratio was not affected by the inhibition of TRPV4 activities at day 2, while a significant decrease in the YAP/TAZ ratio (from 2.6 ± 0.5 to 1.7 ± 0.3) was observed for VICs at day 5 (**Figure 6**A,B). Dual inhibition of YAP/TAZ and TRPV4 activities were performed to further elucidate the relationships between mechanotransduction and calcium signaling in regulating VIC spreading and myofibroblast activation. VIC alignment was not affected by inhibition of the YAP/TAZ nuclear shuttling alone (Figure 6C); however, TRPV4 antagonism alone was sufficient to inhibit cell

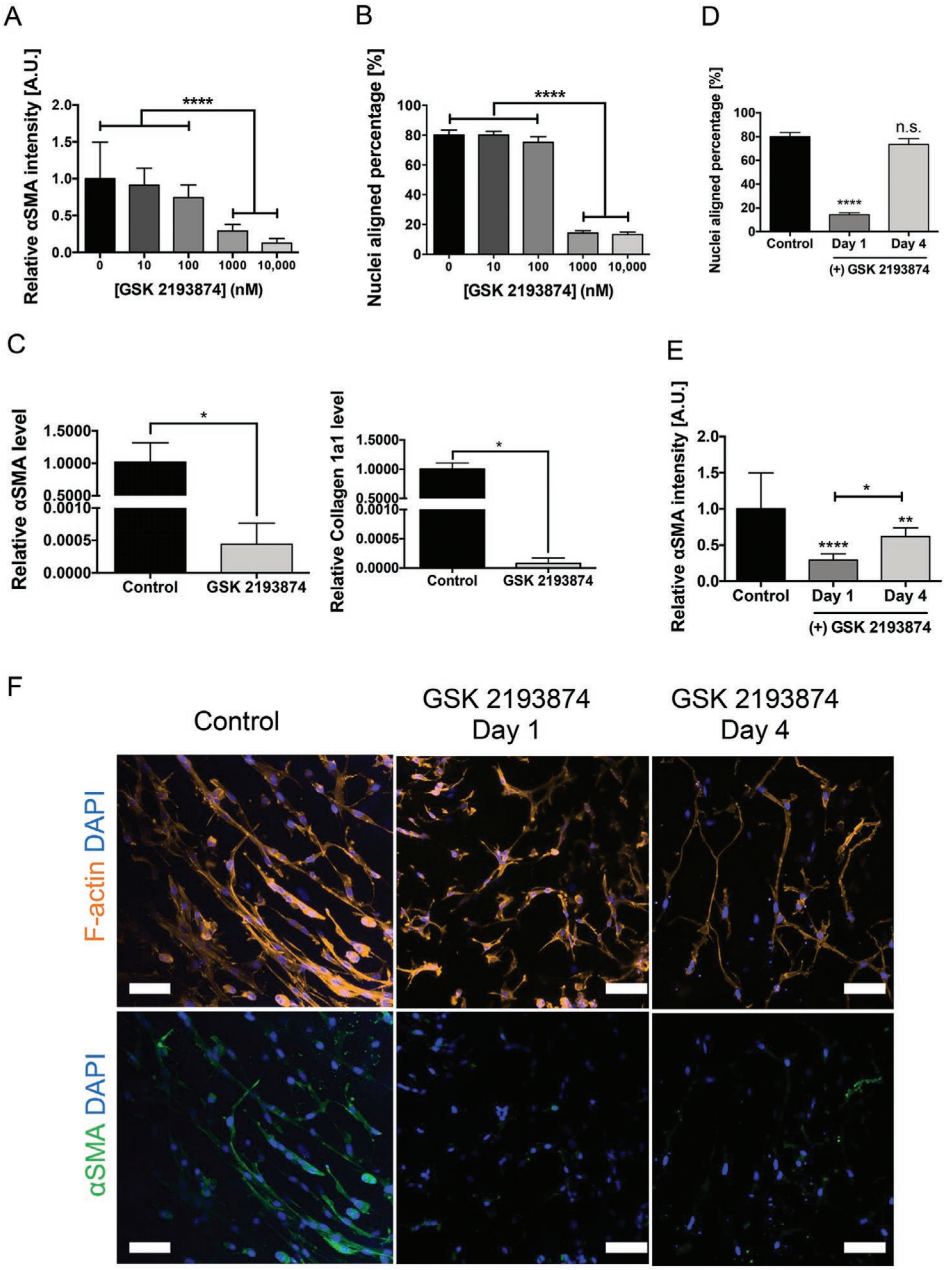

42

Figure 5. TRPV4 activity correlates with VIC spreading and myofibroblast activation. A) Quantification of αSMA intensity of VICs cultured in the high viscoelastic system at Day 5 in response to TPRV4 antagonist (GSK 2193874) treatment (10–10 000 $\times$ 10^{-9} M) at Day 1. B) Quantification of nuclear alignment of VICs cultured in the high viscoelastic system in response to TPRV4 antagonist (GSK 2193874) treatment (10–10 000 $\times$ 10^{-9} M) at Day 5. C) mRNA relative gene expression levels normalized to L30 of key myofibroblast markers, αSMA and COL1A1, for VICs cultured in the high viscoelastic system with or without TRPV4 antagonist (GSK 2193874) treatment (1000 $\times$ 10^{-9} M) at Day 4. D) Quantification of nuclear alignment of VICs cultured in the high viscoelastic system at Day 5 with TPRV4 antagonist (GSK 2193874) treatment (1000 $\times$ 10^{-9} M) added at Day 1 or Day 4. E) Quantification of αSMA intensity at day 5 of VICs cultured in the high viscoelastic system with TPRV4 antagonist (GSK 2193874) treatment (1000 $\times$ 10^{-9} M) added at Day 1 or Day 4. F) Representative immunostaining images of nuclei (blue), F-actin (orange), and αSMA (green) of VICs cultured in the high viscoelastic system at Day 5 with TRPV4 antagonist (GSK 2193874) treatment (1000 $\times$ 10^{-9} M) added at Day 1 or Day 4. Values are plotted as mean $\pm$ standard deviation. n.s.: $p > 0.05$, *: $p < 0.05$, ****: $p < 0.0001$, based on one-way ANOVA. Three biological replicates with three technical replicates in each biological replicate, at least 200 VICs were analyzed per technical replicate. Scale bar = 50 μm.

alignment. Further decreases in VIC spreading and alignment were not observed upon dual inhibition of both YAP/TAZ and TRPV4 activities, compared to single inhibition of TPRV4. Both single inhibition of YAP/TAZ or TPRV4 significantly decreased the αSMA expression of VICs cultured in high viscoelastic hydrogels by 42 $\pm$ 18% and 71 $\pm$ 9%, correspondingly. When

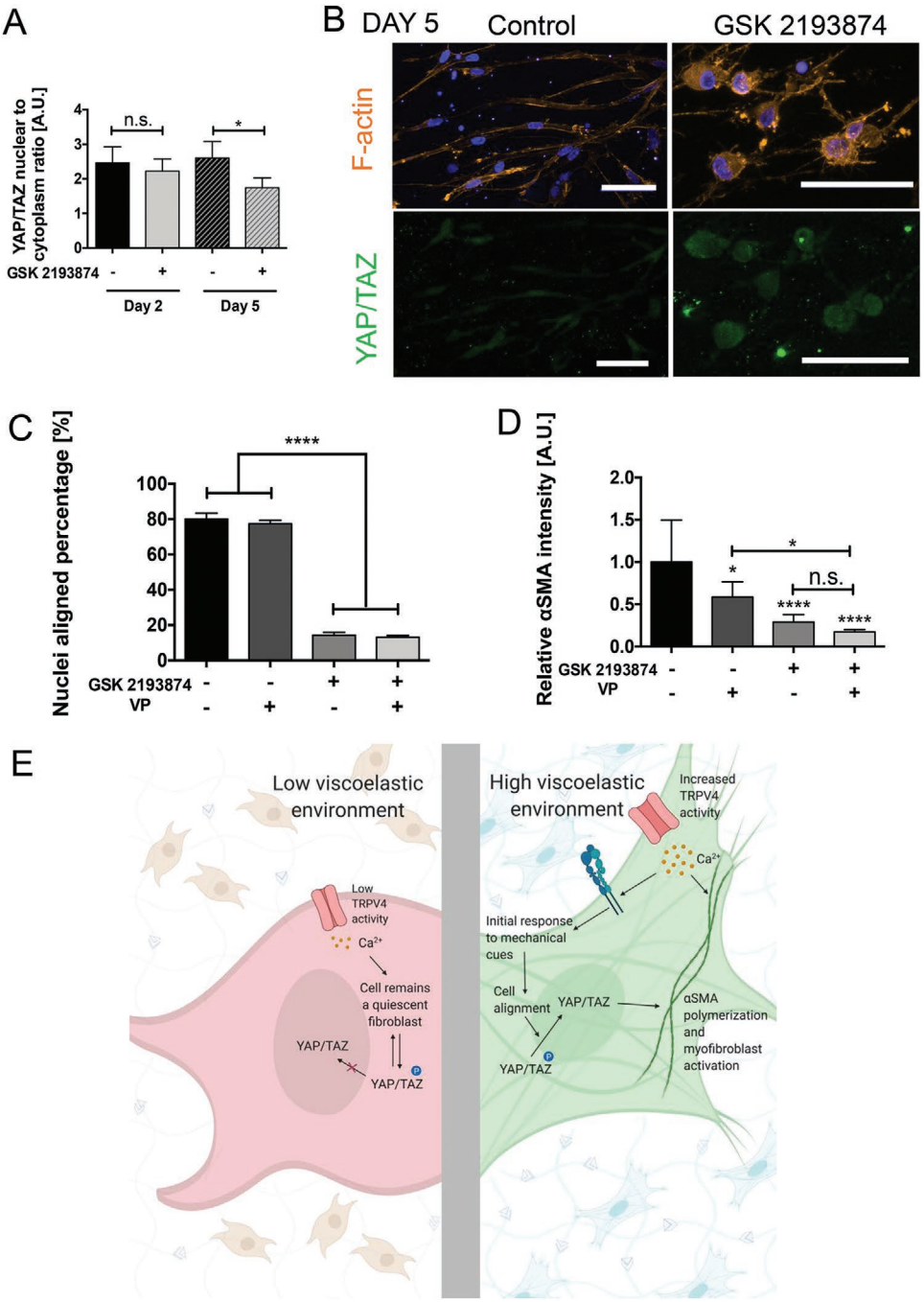

Figure 6. Crosstalk between mechanotransduction and TPRV4 activity in regulating VIC myofibroblast activation. A) Quantification of YAP/TAZ nuclear to cytoplasm ratio for VICs cultured in high viscoelastic system at Day 2 and Day 5 with TRPV4 antagonist (GSK 2193874) treatment (1000×10^{-9} M) at Day 1. B) Representative immunostaining images of nucleus (blue), F-actin (orange), and YAP/TAZ (green) of VIC cultured in high viscoelastic system at Day 5 with TRPV4 antagonist (GSK 2193874) treatment (1000×10^{-9} M) at Day 1. C) Quantification of nuclear alignment of VICs cultured in high viscoelastic system at Day 5 with YAP/TAZ inhibitor (VP) and/or TRPV4 antagonist (GSK 2193874) treatment at Day 1. D) Quantification of αSMA intensity of VICs cultured in high viscoelastic system at Day 5 with YAP/TAZ inhibitor (VP) and/or TRPV4 antagonist (GSK 2193874) treatment at Day 1. E) Schematic for hypothesized mechanism of crosstalk between TRPV4 calcium signaling and YAP/TAZ mechanotransduction in regulating VIC myofibroblast activation. Values are plotted as mean ± standard deviation. n.s.: $p > 0.05$, *: $p < 0.05$, ****: $p < 0.0001$, based on one-way ANOVA. Three biological replicates with three technical replicates in each biological replicate, at least 200 VICs were analyzed per technical replicate. Scale bar = 50 µm.

both YAP/TAZ and TRPV4 activities were inhibited, the expression of αSMA decreased by 83 ± 3% compared to the non-treated control group. The expression level of αSMA upon dual inhibition was significantly lower compared to single inhibition of YAP/TAZ but not by single inhibition of TRPV4 activities (Figure 6D).

3. Discussion

Viscoelasticity has recently emerged as a tissue mechanical property proven to affect cell–matrix interactions and cell fate determination. In this study, a hydrogel systems with boronate bonds, which exhibit fast-relaxing mechanical properties,[31] was exploited to investigate how viscoelasticity can influence VIC myofibroblast activation. VICs reside in a tissue microenvironment where the matrix properties change over time with injury and disease progression. Therefore, an indepth understanding into whether viscoelastic matrix properties can influence changes in the VIC phenotype, in addition to mechanisms related to persistence of VIC myofibroblast activation, might lead to improved medical treatments for aortic valve disease.

VICs are known for regulating valvular tissue homeostasis by transitioning from a quiescent fibroblast phenotype to activated myofibroblast phenotype, characterized by an increase of αSMA stress fibers expression and collagen secretion. The orientation of deposited collagen fibers as determined by cell orientation can significantly alter the tissue mechanical properties and further affect cellular behavior. The specific role that viscoelasticity plays in controlling the orientation and organization of ECM deposition in the valve microenvironment remains unknown. Hence, a covalently adaptable boronate hydrogel systems was used to present encapsulated VICs with different percentage of stress relaxation in their extracellular environment and such systems serve as more physiologically relevant systems to study VIC responses to drug candidates. In biomaterial matrices with the highest percentage of relaxation, rapid spreading was observed in VICs within 1 day postencapsulation, and clear alignment was observed in VICs by day 5. These results indicate that matrix viscoelasticity likely plays a role in promoting VIC spreading and alignment, both of which correlate to tissue homeostasis (Figure 2A,B). Noticeably, the extent of relaxation required for VICs to exhibit an activated myofibroblast phenotype (≈90%) within the boronate hydrogels is significantly higher than ex vivo relaxation measurement of healthy valvular tissue (≈30%). This difference may be due, in part, to other microenvironmental cues (e.g., cytokines) that are present in vivo, but not in vitro. Further characterization of the mechanical properties of valvular tissue, along with changes in the cellular and matrix composition, would help elucidate the relative role of viscoelastic changes compared to other biochemical cues during valve fibrosis. Significant increases in key myofibroblast markers, αSMA and COL1A1, were measured in the aligned VICs at day 5, and expression of these markers were diminished by treatment with FGF-2. The decrease in αSMA and COL1A1 for VICs treated with FGF-2 is consistent with the literature that FGF-2 has antifibrotic effects on a variety of fibroblasts.[44,51–54] Previous work has shown the mechanism of FGF-2 deactivation of VIC myofibroblast is by inhibiting TGF-β signaling pathways.[55] Taken together, these results suggest VIC alignment triggered by viscoelasticity matrix properties can further lead to VIC myofibroblast activation (Figures 2 and 3).

VIC mechanotransduction was also evaluated in hydrogel formulas with different extents of boronate crosslinks, and higher activation was observed for VICs cultured in hydrogels that allowed more stress relaxation, as characterized by YAP/TAZ subcellular localization (Figure 4A,B). These results indicate that viscoelasticity correlates with VIC myofibroblast activation and may suggest a time constant with mechanotransduction. Next, the YAP/TAZ nuclear shuttling mechanism was inhibited, and the corresponding VIC behavior was monitored to further elucidate how mechanotransduction might be involved in viscoelasticity-regulated VIC activation. Upon the inhibition of YAP/TAZ nuclear shuttling, decreased expression of key myofibroblast markers was observed, but VIC alignment remained unaltered. This result indicated that intracellular mechanotransduction processes may be activated after processes that control VIC alignment (Figure 4C–G). Such findings are aligned with prior literature that YAP/TAZ regulated mechanotransduction is involved during VIC myofibroblast activation in response to changes in the dynamic biophysical properties of the microenvironments.[13,56–58] In the wider context of this work, these results suggest that changes in tissue mechanical properties during disease progression might contribute to VIC myofibroblast activation initially and that VIC myofibroblasts further feed back into more mechanical property changes in the valvular tissue.[60] This positive feedback loop might contribute to the irreversibility of advanced fibrotic valve disease, and future studies would benefit from advanced biomaterial systems to study valve fibrosis and screen for pharmaceutical treatments.[61] Even though VP has been identified as a good inhibitor for YAP/TAZ nuclear shuttling, it might not be sufficient to fully inhibit the transcriptional function of YAP/TAZ, and a more in-depth study is needed to better understand the specific mechanisms involved.

In prior published work, the TRPV4 channel has been shown to be mechanoresponsive and regulate the activation of various types of fibroblast, as well as to be a key regulator for stem cell differentiation in a viscoelastic microenvironments.[21,22,29] TRPV4 activities have also been proven to regulate the orientation of collagen fiber deposition.[50] Based on these findings, VIC TRPV4 activity was examined to elucidate whether calcium signaling might regulate VIC spreading, alignment, and myofibroblast activation. VICs cultured in the boronate hydrogel system that allowed the highest levels of stress relaxation exhibited a twofold higher calcium level in the cytoplasm, indicating the calcium influx to the cells through calcium permeable channels, like TRPV4, was increased (Figure S1, Supporting Information). Experiments to inhibit TRPV4 activity were then performed and corresponding cellular responses were monitored. When TRPV4 activity was inhibited at day 1, VIC alignment was disturbed and myofibroblast activation was diminished by day 5, indicating that TPRV4 may be involved in regulating VIC responses to viscoelasticity. Interestingly, when TPRV4 activity was inhibited at day 4, VIC alignment was maintained, but VIC myofibroblast activation was still diminished by day 5, potentially indicating that TPRV4 activity may regulate not only VIC spreading and alignment but also myofibroblast activation (Figure 5). Together with the data from Figures 2 and 4, it is demonstrated that viscoelasticity can promote VIC spreading and alignment correlating with activation of TPRV4 channels. Besides regulating VIC spreading and alignment, TRPV4 activity is still necessary for initiating VIC myofibroblast activation after cell alignment is established. This suggests that after VIC alignment is formed, the remaining activated TRPV4 signaling can crosstalk with mechanotransduction

to further activate VICs into a myofibroblastic phenotype, as inhibition of the YAP/TAZ nuclear shuttling mechanism also diminishes VIC fibrotic activation. It was further hypothesized that the increase of viscoelasticity during the initial phase of wound healing or disease progression may potentially lead to VIC spreading and alignment via TPRV4 channels. Subsequently, TPRV4 activities can be turned off or internalized by other mechanism,[62] potentially related to the crosstalk with valvular endothelial cells (VECs), while tissue homeostasis is maintained.[49] If TPRV4 channels are misregulated, further myofibroblast activation would be triggered, which might lead to valve leaflet tissue fibrosis.[17]

Further manipulation of YAP/TAZ and TRPV4 signaling was conducted to further investigate how these two signaling pathways may work together to regulate VIC myofibroblast activation. YAP/TAZ nuclear to cytoplasm ratio was monitored at different time points upon TRPV4 inhibition. YAP/TAZ subcellular localization was not influenced at 1 day post TPRV4 antagonist treatment, but was significantly decreased from 2.6 ± 0.5 to 1.7 ± 0.3 at 4 days post TPRV4 inhibition (Figure 6A,B), indicating that crosstalk between TPRV4 signaling and YAP/TAZ signaling is indirect, likely via integrin clustering and cell morphological changes.[63] When YAP/TAZ and TRPV4 activities were both inhibited, VIC cell spreading, alignment, and myofibroblast activation were similar, compared to the TRPV4 single inhibited condition but were significantly lower compared to YAP/TAZ single inhibition condition. This result indicates that TRPV4 signaling may be partially involved in the same signaling pathway with mechanotransduction and is upstream of YAP/TAZ nuclear shutting. Single inhibition of the YAP/TAZ nuclear shuttling mechanism led to higher levels of VIC spreading, alignment, and myofibroblast activation compared to TPRV4 single inhibition, suggesting that TRPV4 calcium signaling can also regulate VIC behavior independent of YAP/TAZ subcellular localization (Figure 6C,D).

Based on these data, a hypothesized potential signaling crosstalk mechanism between YAP/TAZ mechanotransduction and TRPV4 calcium signaling while regulating VIC myofibroblast activation has been proposed (Figure 6E). We put forth the notion that calcium channels (e.g., TRPV4) are more open in a highly viscoelastic microenvironment (i.e., stress relaxing) due to cell spreading and membrane stretching compared to cells cultured in materials that do not allow for relaxation. Activated calcium channels can initiate cytoplasmic signaling which could act on αSMA production and/or assemble independently of mechanotransduction and also partially influence the mechanotransduction process likely via integrin clustering, cell morphological changes, and cell alignment.[62] A range of mechanisms have been identified for different cell types regarding the crosstalk between YAP/TAZ and TRPV4.[20,46,48] However, the specific mechanism for VICs is still largely unknown, and future experiments should be designed to elucidate the specific regulators that are involved in this crosstalk mechanism. For instance, nuclear factor of activated T-cells (NFAT) have been indicated as potential downstream regulators of TRPV4 calcium signaling while regulating myofibroblast activation.[64] Nitric oxide (NO) has been shown to be involved in the crosstalk between VIC and VEC, with the expression of NO linked to TPRV4 activities.[19,65,66] Additionally, the PI3K pathway has been linked to VIC mechanotransduction and recently shown to interact with TRPV4 to facilitate myofibroblast activation and regulate profibrotic response.[67] The PI3K pathway, which has been found to positively regulate YAP/TAZ signaling, might be one possible link between TRPV4 signaling and YAP/TAZ activity.[68,69] Overall, this study uses a hydrogel material system with tunable viscoelastic properties to better understand how time varying matrix properties affect VIC mechanosensing through mechanisms that involve YAP/TAZ and TRPV4 signaling pathways. Because this work relied on porcine-VICs, the aforementioned findings need to be validated using VICs isolated from human tissue because of potential difference in the magnitude of their cellular responses. Once established, the materials reported and the 3D culture methods developed in this work should prove useful for studying valve fibrosis and provide insights as to potential targets for pharmaceutical treatments.

4. Conclusion

As a time-dependent mechanical property, viscoelasticity arises as an important matrix property that influences cell behavior and may be related to disease progression. In this manuscript, covalently adaptable networks that incorporate a range of reversible boronate bonds were exploited to create materials with a wide range of stress relaxation properties. These materials were used for 3D VIC culture and to investigate the effect of viscoelasticity on VIC spreading, alignment, and myofibroblast activation, early markers of aortic valve stenosis. VIC spreading and alignment correlated with higher extents of matrix viscoelasticity and stress relaxation by activating TPRV4 channels. Both TRPV4 and YAP/TAZ signaling regulated VIC alignment, followed by myofibroblast activation. A potential crosstalk between viscoelasticity, calcium signaling, and mechanotransduction is proposed with the overall goal of providing new insight into potential target for valvular tissue fibrosis treatment.

5. Experimental Section

Materials Synthesis Procedures: Octa-arm PEG-hydroxyl (M_n = 20 kg mol^{-1}, tripentaerythritol core) and octa-arm PEG-amine (M_n = 20 kg mol^{-1}, hexaglycerol core or tripentaerythritol core) were purchased from JenKem Technology USA. DBCO (dibenzylcyclooctyne) acid, 3-azidopropinoic acid, and azido propylamine were purchased from Click Chemistry Tools. All chemicals for peptide synthesis were purchased from Chem-Impex International Inc. All other chemicals were purchased from Sigma-Aldrich or Fisher and used as received unless otherwise noted.

^{1}H NMR and ^{13}C NMR were recorded on a 400 MHz Bruker AVANCE spectrometer. The residual undeuterated solvent peaks were used for references (7.26 ppm for $CDCl_3$,). Octa-arm PEG-azide, azido-GRGDS, octa-arm PEG DBCO, octa-arm PEG-azide/ Fluorophenylboronic acid (FPBA), octa-arm PEG-azide/ND, and their intermediate products were synthesized as previously described in detail.[31] Importantly, for both octa-arm PEG-azide/FPBA and octa-arm PEG azide/ND, 2 arms were first functionalized with azide group and confirmed through a TNBS (2,4,6-trinitrobenzene sulfonic acid) assay before the remaining 6 arms were functionalized with either FPBA or ND, respectively.

Rheology Measurements of Hydrogels: Rheology experiments were performed on a DHR-3 rheometer (TA instrument) with an 8 mm stainless steel upper plate, and the temperature was controlled by a

Peltier bottom plate. Inertial calibration and motor adjustment were performed before each experiment. Frequency sweep experiments were performed at 1% strain (within the linear viscoelastic regime as predetermined from strain sweep experiments) from 100 to 0.01 rad s^{-1}. Optically thin hydrogels were formed by mixing appropriate volumes of PEG macromer solutions (add wt% of stocks) to reach the desired final polymer content and stoichiometry as summarized in Table S1 (Supporting Information). Hydrogels with a thickness of 250 µm were formed in a rubber mold. After swollen in culture media for 24 h, the hydrogel constructs were transferred to between a Quartz bottom plate and an 8 mm diameter stainless steel upper plate. The relaxation curve was monitored using a dynamic frequency sweep at 1% strain.

VIC Isolation, Culture, and Encapsulation: Primary VICs were isolated from fresh male porcine hearts (Hormel) as previously described.[13,44,59] Briefly, porcine aortic valve leaflets were excised from the hearts, rinsed in Earle's Balanced Salt Solution (Life Technologies) with 1% penicillin-streptomycin (Life Technologies) and 0.5 mg mL^{-1} fungizone (Life Technologies) and subsequently incubated in a collagenase solution (250 units mL^{-1}, Worthington) for 30 min at 37 °C. Endothelial cells were removed by vortexing and centrifugation, followed by another incubation in collagenase solution for 60 min at 37 °C. Filtration of the solution with a 100 µm cell strainer was conducted to separate VICs from the remaining extracellular matrix. Next, VICs were pelleted by centrifugation and then resuspended in growth media (Media 199, Gibco Life Technology #11150-059) supplemented with 15% fetal bovine serum (FBS, Life Technologies), 2% penicillin-streptomycin, and 0.5 mg mL^{-1} fungizone). Fibroblast growth factor 2 (FGF-2), YAP/TAZ inhibitor (3×10^{-6} M, Verteporfin), and TRPV4 antagonist (GSK 2193874) were supplemented as stated (FGF-2, Sigma-Aldrich; Verteporfin, Sigma; GSK 2193874, Tocris). The isolated VICs were expanded on tissue culture polystyrene (TCPS) until 80% confluence and frozen down in FBS containing 20% dimethyl sulfoxide and stored in liquid nitrogen as Passage 1 (P1). P2 to P4 VICs were generated by expanding the P1 stock in growth media (Dulbecco's modified eagle medium supplemented with 15% FBS, 50 U mL^{-1} penicillin, 50 mg mL^{-1} streptomycin, and 1 mg mL^{-1} fungizone), and P2 to P4 VICs were used in all the reported experiments. VICs were cultured on TCPS in growth media at 5×10^5 cells cm^{-2} for 2 days prior to encapsulation in hydrogels. VICs were then trypsinized, pelleted, and resuspended into 10% FBS media to a desired concentration such that the final density of encapsulated VICs was 10 million cells mL^{-1}. For nonrelaxing gels, stock solutions of octa-arm PEG-azide (20 wt% stock dissolved in PBS), azido-GRGDS (100×10^{-3} M), and the VIC suspension were gently mixed, and then the octa-arm PEG-DBCO solution (10 wt% stock) was quickly added. The mixture was pipetted several times and quickly transferred to a syringe barrel. After 10 min, the construct was equilibrated in prewarmed media. For relaxing gels, stock solutions of octa-arm PEG-DBCO (10 wt% stock), azido-GRGDS (100×10^{-3} M), and the cell suspension were gently mixed. The mixture was transferred to a syringe barrel. Then octa-arm PEG-azide/FPBA and octa-arm PEG-azide/ND (20 wt% stock) were sequentially added to reach the desired final polymer content as summarized in Table S1 (Supporting Information). The mixture was quickly triturated several times after adding each component. Constructs were allowed to gel at 37 °C for 15 min and were then placed into prewarmed media. Media was changed the first day after encapsulation and every other day afterward.

Live/Dead Assay: Hydrogels were incubated in phenol red free Media 199 (supplemented with 10% FBS) with 0.5×10^{-6} M calcein AM and 4.0×10^{-6} M ethidium homodimer for 30 min per manufacturer's protocol. Hydrogels were imaged using a high-content imaging system (Operetta; Perkin Elmer). Viability was determined using a membrane integrity assay, and by counting live cells (green) and dead cells (red) in images stacked from maximum intensity projections (step size 5 µm, total thickness ≈200 µm).

Immunostaining: VICs were fixed in 4% paraformaldehyde for 1 h at room temperature, rinsed in PBS twice, and then permeabilized using 0.1% TritonX-100 in PBS for 2 h. Next, samples were blocked in PBS with 5% bovine serum albumin (BSA) for 2 h at room temperature to minimize nonspecific protein binding. Anti-αSMA (1:200, mouse, Abcam) primary antibodies in 5% BSA were applied to samples and incubated at 4 °C overnight with gentle shaking. Primary antibodies were removed by rinsing in PBST (0.5 wt% Tween-20 in PBS) for at least 3 h with five times buffer change. Samples were then incubated at 4 °C with secondary antibodies (1:1000, goat antirabbit AlexaFluor 488; goat antimouse AlexaFluor 647, invitrogen), phalloidin (1:300, Sigma-Aldrich) and DAPI (1 mg mL^{-1}; Sigma) in PBS with 1% BSA overnight. The secondary antibody solution was removed, and the samples were rinsed for 3 h with five times buffer change with PBST. All immunostained samples were stored in PBS at 4 °C until imaging (LSM 710, Zeiss).

Cytoplasmic Calcium Intensity Measurement: VIC cytoplasmic calcium intensity was measured by Fluo-4 calcium imaging kit (Thermo Fisher). Hydrogel constructs with VICs encapsulated were incubated in phenol red free Media 199 (supplemented with 10% FBS) with Fluo-4 at 1:1000 dilution at 37 °C for 30 min per manufacturer's protocol. Excess of fluo-4 was removed by rinse with phenol red free Media 199 without Fluo-4. Hydrogels were then imaged using a high-content imaging system (Operetta; Perkin Elmer) and intensity of calcium was measured by Harmony software that is associated with imaging system.

Image Acquisition and Analysis: Immunofluorescence images were taken using a laser scanning confocal microscope (Zeiss, LSM710) with a Plan-Apochromat 20 × (NA = 1.0) water objective. Images were quantified using Imaris software (Bitplane). 3D views were first reconstructed from z-stack images (step size 1.5 µm). The cell and the nucleus were determined from the rhodamine and the DAPI channels, respectively. Cell orientation was determined by the orientation of cell nucleus in Image J as described in detail elsewhere.[16] Specially, the orientation of nucleus was identified by fitting an oval to the nucleus and measuring the orientation of this oval. Nucleus that had an orientation within a 10° angle of the most frequent orientation was defined as nuclear alignment of the VICs.

The YAP/TAZ nuclear to cytosolic ratio was calculated based on the following formula.

$$\text{YAP/TAZ } nuc/cyt \text{ } ratio = \frac{I_{nuc} / V_{nuc}}{\left[\frac{I_{cell} - I_{nuc}}{V_{cell} - V_{nuc}}\right]} \quad (1)$$

where I_{nuc} and I_{cell} are the total intensities of the YAP/TAZ signal inside the nucleus and the cell, respectively, and V_{nuc} and V_{cell} are the volumes of the nucleus and the cell, respectively.

mRNA Isolation and Quantitative RT-qPCR Assessment of Gene Expression: Total mRNA was isolated from hydrogels using RNeasy Micro Kit (Qiagen) and eluted in RNAse free water. The mRNA concentration and quality were assessed with a ND-1000 Nanodrop Spectrophotometer. For RT-qPCR, cDNA was synthesized with the iScript Reverse Transcription Supermix kit (Bio-Rad) and an Eppendorf Mastercycler. Relative mRNA expression levels were measured using SYBR Green reagents (Bio-Rad) using an iCycler machine (Bio-Rad), normalizing to the housekeeping gene (ribo- somal protein L30). Custom primers are presented as following

Gene names	Forward primer (5'-3')	Reverse primer (5'-3')
L30	GCTGGGGTACAAGCAGACTC	AGATTTCCTCAAGGCTGGGC
αSMA	GCAAACAGGAATACGATGAAGCC	AACACATAGGTAACGAGTCAGAGC
COL1A1	GGGCAAGACAGTGATTGAATACA	GGATGGAGGGAGTTTACAGGAA

Statistical Analysis: For each experiment, at least three biological replicates were performed using different pools of male porcine hearts with three technical replicates in each biological replicate. Each pool of male porcine VICs consists of at least 10 porcine hearts. For cell analyses, at least 200 cells were assessed per condition per technical replicate. Data were compared using one-way ANOVAs and Bonferroni post-tests in Prism 7 (GraphPad Software, Inc) unless otherwise stated. Data are presented as mean ± standard deviation. Significance levels

were indicated by *, **, ***, and **** for $p < 0.05$, 0.01, 0.001, and 0.0001, respectively.

Supporting Information

Supporting Information is available from the Wiley Online Library or from the author.

Acknowledgements

The authors would like to thank Tova Ceccato for helpful discussions. D.B. acknowledges support from the American Heart Association (No. 20PRE35200068). The authors would also like to acknowledge support from the National Institutes of Health (Grant Nos. R01 HL132353 and R01 HL142935).

Conflict of Interest

The authors declare no conflict of interest.

Keywords

3D hydrogels, boronate chemistries, mechanotransduction, myofibroblasts, valvular interstitial cells

Received: July 28, 2020
Published online: September 13, 2020

[1] B. Jian, N. Narula, Q.-y. Li, E. R. Mohler, R. J. Levy, *Ann. Thorac. Surg.* **2003**, *75*, 457.
[2] R. B. Hinton, K. E. Yutzey, *Annu. Rev. Physiol.* **2011**, *73*, 29.
[3] V. L. Roger, A. S. Go, D. M. Lloyd-Jones, R. J. Adams, J. D. Berry, T. M. Brown, M. R. Carnethon, S. Dai, G. De Simone, E. S. Ford, C. S. Fox, H. J. Fullerton, C. Gillespie, K. J. Greenlund, S. M. Hailpern, J. A. Heit, P. M. Ho, V. J. Howard, B. M. Kissela, S. J. Kittner, D. T. Lackland, J. H. Lichtman, L. D. Lisabeth, D. M. Makuc, G. M. Marcus, A. Marelli, D. B. Matchar, M. M. McDermott, J. B. Meigs, C. S. Moy, D. Mozaffarian, M. E. Mussolino, G. Nichol, N. P. Paynter, W. D. Rosamond, P. D. Sorlie, R. S. Stafford, T. N. Turan, M. B. Turner, N. D. Wong, J. Wylie-Rosett, American Heart Association Statistics Committee and Stroke Statistics Subcommittee, *Circulation* **2011**, *123*, 18.
[4] R. A. Nishimura, C. M. Otto, R. O. Bonow, B. A. Carabello, J. P. Erwin, L. A. Fleisher, H. Jneid, M. J. Mack, C. J. McLeod, P. T. O'Gara, V. H. Rigolin, T. M. Sundt 3rd, A. Thompson, *J. Am. Coll. Cardiol.* **2017**, *70*, 252.
[5] A. C. Liu, V. R. Joag, A. I. Gotlieb, *Am. J. Pathol.* **2007**, *171*, 1407.
[6] G. A. Walker, K. S. Masters, D. N. Shah, K. S. Anseth, L. A. Leinwand, *Circ. Res.* **2004**, *95*, 253.
[7] X. Wang, M. Ali, C. Lacerda, *Bioengineering* **2018**, *5*, 69.
[8] H. Wang, S. M. Haeger, A. M. Kloxin, L. A. Leinwand, K. S. Anseth, *PLoS One* **2012**, *7*, e39969.
[9] H. Wang, L. A. Leinwand, K. S. Anseth, *Nat. Rev. Cardiol.* **2014**, *11*, 715.
[10] S. Sell, R. E. Scully, *Am. J. Pathol.* **1965**, *46*, 345.
[11] B. Hinz, G. Gabbiani, *F1000 Biol. Rep.* **2010**, *2*, 78.
[12] M. D. Davidson, J. A. Burdick, R. G. Wells, *Adv. Healthcare Mater.* **2020**, *9*, 1901682.
[13] H. Ma, A. R. Killaars, F. W. DelRio, C. Yang, K. S. Anseth, *Biomaterials* **2017**, *131*, 131.
[14] N. J. Driessen, R. A. Boerboom, J. M. Huyghe, C. V. Bouten, F. P. Baaijens, *J. Biomech. Eng.* **2003**, *125*, 549.
[15] A. C. Zeigler, W. J. Richardson, J. W. Holmes, J. J. Saucerman, *J. Mol. Cell. Cardiol.* **2015**, *93*, 73.
[16] J. H. C. Wang, F. Jia, T. W. Gilbert, S. L. Y. Woo, *J. Biomech.* **2003**, *36*, 97.
[17] C. K. Thodeti, S. Paruchuri, J. G. Meszaros, *Channels* **2013**, *7*, 211.
[18] L. Zhan, J. Li, *Gene* **2018**, *642*, 1.
[19] J. Richards, I. El-Hamamsy, S. Chen, Z. Sarang, P. Sarathchandra, M. H. Yacoub, A. H. Chester, J. T. Butcher, *Am. J. Pathol.* **2013**, *182*, 1922.
[20] H. P. Lee, R. Stowers, O. Chaudhuri, *Nat. Commun.* **2019**, *10*, 529.
[21] R. K. Adapala, R. J. Thoppil, D. J. Luther, S. Paruchuri, J. G. Meszaros, W. M. Chilian, C. K. Thodeti, *J. Mol. Cell. Cardiol.* **2013**, *54*, 45.
[22] S. O. Rahaman, D. J. Tschumperlin, A. Mitchell, S. O. Rahaman, L. M. Grove, S. Paruchuri, B. D. Southern, S. Abraham, K. A. Niese, R. G. Scheraga, S. Ghosh, C. K. Thodeti, D. X. Zhang, M. M. Moran, W. P. Schilling, D. J. Tschumperlin, M. A. Olman, *J. Clin. Invest.* **2014**, *124*, 5225.
[23] S. Sharma, R. Goswami, M. Merth, J. Cohen, K. Y. Lei, D. X. Zhang, S. O. Rahaman, *Am. J. Physiol.: Cell Physiol.* **2017**, *312*, C562.
[24] C. K. Thodeti, B. Matthews, A. Ravi, A. Mammoto, K. Ghosh, A. L. Bracha, D. E. Ingber, *Circ. Res.* **2009**, *104*, 1123.
[25] J. Liao, I. Vesely, *Ann. Biomed. Eng.* **2004**, *32*, 977.
[26] O. Chaudhuri, L. Gu, M. Darnell, D. Klumpers, S. A. Bencherif, J. C. Weaver, N. Huebsch, D. J. Mooney, *Nat. Commun.* **2015**, *6*, 6365.
[27] M. Darnell, S. Young, L. Gu, N. Shah, E. Lippens, J. Weaver, G. Duda, D. Mooney, *Adv. Healthcare Mater.* **2016**, *6*, 1601185.
[28] E. A. Hushka, F. M. Yavitt, T. E. Brown, P. J. Dempsey, K. S. Anseth, *Adv. Healthcare Mater.* **2020**, *9*, 1901214.
[29] O. Chaudhuri, L. Gu, D. Klumpers, M. Darnell, S. A. Bencherif, J. C. Weaver, N. Huebsch, H.-P. Lee, E. Lippens, G. N. Duda, D. J. Mooney, *Nat. Mater.* **2015**, *15*, 326.
[30] A. R. Cameron, J. E. Frith, J. J. Cooper-White, *Biomaterials* **2011**, *32*, 5979.
[31] S. Tang, H. Ma, H.-C. Tu, H.-R. Wang, P.-C. Lin, K. S. Anseth, *Adv. Sci.* **2018**, *5*, 1800638.
[32] J. A. Stella, J. Liao, M. S. Sacks, *J. Biomech.* **2007**, *40*, 3169.
[33] C. E. Eckert, R. Fan, B. Mikulis, M. Barron, C. A. Carruthers, V. M. Friebe, N. R. Vyavahare, M. S. Sacks, *Acta Biomater.* **2013**, *9*, 4653.
[34] I. A. Marozas, K. S. Anseth, J. J. Cooper-white, *Biomaterials* **2019**, *223*, 119430.
[35] C. J. Kloxin, C. N. Bowman, *Chem. Soc. Rev.* **2013**, *42*, 7161.
[36] D. D. McKinnon, D. W. Domaille, J. N. Cha, K. S. Anseth, *Adv. Mater.* **2014**, *26*, 865.
[37] Y. Guan, Y. Zhang, *Chem. Soc. Rev.* **2013**, *42*, 8106.
[38] C. Zhang, M. D. Losego, P. V. Braun, *Chem. Mater.* **2013**, *25*, 3239.
[39] C. C. Deng, W. L. A. Brooks, K. A. Abboud, B. S. Sumerlin, *ACS Macro Lett.* **2015**, *4*, 220.
[40] S. H. Hong, M. Shin, E. Park, J. H. Ryu, J. A. Burdick, H. Lee, *Adv. Funct. Mater.* **2019**, 1908497.
[41] M. E. Smithmyer, C. C. Deng, S. E. Cassel, P. J. Levalley, B. S. Sumerlin, A. M. Kloxin, *ACS Macro Lett.* **2018**, *7*, 1105.
[42] Z. Gong, S. E. Szczesny, S. R. Caliari, E. E. Charrier, O. Chaudhuri, X. Cao, Y. Lin, R. L. Mauck, P. A. Janmey, J. A. Burdick, V. B. Shenoy, *Proc. Natl. Acad. Sci. USA* **2018**, *115*, E2686.
[43] J. C. Kim, M. J. Son, S. H. Woo, *Arch. Biochem. Biophys.* **2018**, *659*, 33.
[44] Y. Tan, H. Huang, D. C. Ayers, J. Song, *ACS Cent. Sci.* **2018**, *4*, 971.
[45] C. J. O'Conor, H. A. Leddy, H. C. Benefield, W. B. Liedtke, F. Guilak, *Proc. Natl. Acad. Sci. USA* **2014**, *111*, 1316.

[46] M. Cheung, W. Bao, D. J. Behm, C. A. Brooks, M. J. Bury, S. E. Dowdell, H. S. Eidam, R. M. Fox, K. B. Goodman, D. A. Holt, D. Lee, T. J. Roethke, R. N. Willette, X. Xu, G. Ye, K. S. Thorneloe, *ACS Med. Chem. Lett.* **2017**, *8*, 549.
[47] S. Sharma, R. Goswami, D. X. Zhang, S. O. Rahaman, *J. Cell. Mol. Med.* **2019**, *23*, 761.
[48] P. K. Randhawa, A. S. Jaggi, *Basic Res. Cardiol.* **2015**, *110*, 54.
[49] C. L. Gilchrist, H. A. Leddy, L. Kaye, N. D. Case, K. E. Rothenberg, D. Little, W. Liedtke, B. D. Hoffman, F. Guilak, *Proc. Natl. Acad. Sci. USA* **2019**, *116*, 1992.
[50] S. Baratchi, P. Keov, W. G. Darby, A. Lai, K. Khoshmanesh, P. Thurgood, P. Vahidi, K. Ejendal, P. McIntyre, *Front. Pharmacol.* **2019**, *9*, 1.
[51] P. D. Arora, M. Di Gregorio, P. He, C. A. McCulloch, *J. Cell Sci.* **2017**, *130*, 2196.
[52] R. Masuyama, J. Vriens, T. Voets, Y. Karashima, G. Owsianik, R. Vennekens, L. Lieben, S. Torrekens, K. Moermans, A. Vanden Bosch, R. Bouillon, B. Nilius, G. Carmeliet, *Cell Metab.* **2008**, *8*, 257.
[53] S. T. Gould, E. E. Matherly, J. N. Smith, D. D. Heistad, K. S. Anseth, *Biomaterials* **2014**, *35*, 3596.
[54] B. C. W. Groenendijk, B. P. Hierck, J. Vrolijk, M. Baiker, M. J. B. M. Pourquie, A. C. Gittenberger-De Groot, R. E. Poelmann, *Circ. Res.* **2005**, *96*, 1291.
[55] H. Wang, L. A. Leinwand, K. S. Anseth, *FASEB J.* **2014**, *28*, 4551.
[56] Y. Zhao, T. Montminy, T. Azad, E. Lightbody, Y. Hao, S. SenGupta, E. Asselin, C. Nicol, X. Yang, *Mol. Cancer Res.* **2018**, *16*, 1046.
[57] L. M. Grove, M. L. Mohan, S. Abraham, R. G. Scheraga, B. D. Southern, J. F. Crish, S. V. N. Prasad, M. A. Olman, *Sci. Signal.* **2019**, *12*, eaau1533.
[58] C. M. Johnson, M. N. Hanson, S. C. Helgeson, *J. Mol. Cell. Cardiol.* **1987**, *19*, 1185.
[59] A. Gonzalez Rodriguez, M. E. Schroeder, C. J. Walker, K. S. Anseth, *APL Bioeng.* **2018**, *2*, 046104.
[60] F. J. Schoen, *Circulation* **2008**, *118*, 1864.
[61] C. M. Otto, B. Prendergast, *N. Engl. J. Med.* **2014**, *371*, 744.
[62] S. Baratchi, P. Keov, W. G. Darby, A. Lai, K. Khoshmanesh, P. Thurgood, P. Vahidi, K. Ejendal, P. McIntyre, *Front. Pharmacol.* **2019**, *9*, 1.
[63] P. D. Arora, M. Di Gregorio, P. He, C. A. McCulloch, *J. Cell Sci.* **2017**, 1*30*, 2196.
[64] R. Masuyama, J. Vriens, T. Voets, Y. Karashima, G. Owsianik, R. Vennekens, L. Lieben, S. Torrekens, K. Moermans, A. Vanden Bosch, R. Bouillon, B. Nilius, G. Carmeliet, *Cell Metab.* **2008**, *8*, 257.
[65] S. T. Gould, E. E. Matherly, J. N. Smith, D. D. Heistad, K. S. Anseth, *Biomaterials* **2014**, *35*, 3596.
[66] B. C. W. Groenendijk, B. P. Hierck, J. Vrolijk, M. Baiker, M. J. B. M. Pourquie, A. C. Gittenberger-De Groot, R. E. Poelmann, *Circ. Res.* **2005**, *96*, 1291.
[67] H. Wang, L. A. Leinwand, K. S. Anseth, *FASEB J.* **2014**, *28*, 4551.
[68] Y. Zhao, T. Montminy, T. Azad, E. Lightbody, Y. Hao, S. SenGupta, E. Asselin, C. Nicol, X. Yang, *Mol. Cancer Res.* **2018**, *16*, 1046.
[69] L. M. Grove, M. L. Mohan, S. Abraham, R. G. Scheraga, B. D. Southern, J. F. Crish, S. V. N. Prasad, M. A. Olman, *Sci. Signal.* **2019**, *3*, 1.